Synergistic effects of metakaolin and limestone on early hydration kinetics, strength development, and microstructure of low water-to-binder ratio

Case Studies in Construction Materials 24 (2026) e06210

Contents lists available at ScienceDirect

Case Studies in Construction Materials

journal homepage: www.elsevier.com/locate/cscm

Synergistic effects of metakaolin and limestone on early hydration kinetics, strength development, and microstructure of low water-to-binder ratio cement composites

Peimin Zhan [a], Xuan Sun [a], Dongdong Wang [a], Dapeng Wang [a], Weiwei Lin [a], Xuqun Lin [b,*], Juan Wang [c,*], Vivian W.Y. Tam [d]

[a] CCCC Shanghai Harbor Engineering Design & Research Institute Co., Ltd, Shanghai 201804, China
[b] School of Civil and Environmental Engineering, University of Technology Sydney, NSW 2007, Australia
[c] Department of Architecture and Civil Engineering, Chalmers University of Technology, Gothenburg 41296, Sweden
[d] School of Engineering, Design and Built Environment, Western Sydney University, NSW 2751, Australia

ARTICLE INFO

Keywords:
Hydration
Metakaolin
Microstructural analysis
Synergistic effects

ABSTRACT

Metakaolin (MK) and limestone (LS) have attracted attention as a cement replacement for enhancing mechanical and durability properties. The hydration and strength development of MK-LS-cement composites with low water/biner ratio remained unexplored. This study investigated early hydration and strength of binders with MK, limestone (LS), and their combination at a low water/binder ratio of 0.16. Samples containing 13.4 wt% MK and 6.6 wt% LS (C+LSMK) showed comparable hydration heat and 3-day strength to the reference, while 20 wt% LS (C+LS) yielded the lowest hydration heat and early mechanical strengths. XRD indicated greater hemi-carboaluminate and monocarboaluminate formation in C + LSMK, supported by TG/DTG evidence of portlandite consumption. BJH analysis revealed higher capillary pore volume in C + LSMK. Hydration kinetic modelling confirmed that MK enhanced hydration through filler effects and pozzolanic reactions. These findings provided new insights into the synergistic effects of MK and LS in low w/b cement systems, advancing the design of high-performance, low-carbon cementitious materials.

1. Introduction

In recent decades, the rapid growth of the urbanisation and infrastructure development has led to a substantial increase in the global demand for cement and concrete [1,2]. However, cement manufacturing is widely recognised as one of the most energy-intensive and environmentally burdensome industrial processes, owing to the extensive consumption of natural resources, high fossil fuel usage, and the calcination of limestone during clinker production. These processes are responsible for the significant greenhouse gas emissions, accounting for approximately 8% of the global CO_2 emissions [3–5]. Furthermore, construction materials are emerging with higher requirements on environmental protection and improved durability and mechanical properties on the concrete structures. As a result, the explorations of using supplementary cementitious materials (SCMs) to partially replace cement have attracted considerable attention [6–8], including silica fume [9,10], steel slag [11,12], recycled concrete powder [13,14], and

* Corresponding authors.
E-mail addresses: Xuqun.lin@uts.edu.au (X. Lin), juanw@chalmers.se (J. Wang).

https://doi.org/10.1016/j.cscm.2026.e06210
Received 8 March 2026; Received in revised form 13 May 2026; Accepted 1 June 2026
Available online 2 June 2026

rice husk ash [15,16].

Zhang et al. [17] reported that using 4 wt% silica fume to replace cement reduced the chloride diffusion coefficient by 32.32% when compared to the reference mix, being attributed to the proper filler effects and a denser cementitious microstructure due to silica fume addition. Sun et al. [18] explored the effects of steel slag with different particle sizes on the slag-cement composites at 30 wt% cement replacement. They found that samples with ultra-fine steel slag (<10 μm) remained similar 28-day compressive strength when compared to the reference mix, while samples with coarser-size steel slag (<100 μm) exhibited 24.9% compressive strength reduction, highlighting the role of finer-size slag in remaining the compressive strength for samples with 30 wt% cement replacement. He et al. [19] utilised up to 15 wt% rice husk ash (<25.4 μm) as cement replacement, observing that mortar samples with 5 wt% rice husk ash had a similar 28-day compressive strength when compared to the reference mix. They mentioned that the addition of 5 wt% rice husk ash also slightly reduced the hydration heat by 6.4%, preventing the early cracking of the mortar samples. Additionally, Khedher et al. [20] concluded that up to 20 wt% red mud as cement replacement did not lower the 28-day mechanical properties of read mud-cement composites when compared to the control. Furthermore, Hamad et al. [21] mentioned that using FA to partially replace cement could improve the water absorption and resistance against aggressive-ion ingress, due to its high pozzolanic reactivity enhancing microstructure of the FA-cement composites. Overall, the applications of SCMs could improve both mechanical and durability properties of the cementitious composites, while lowering the carbon footprint for sustainable concrete designs.

Metakaolin (MK), produced based on the high-temperature calcination of kaolinite, has been considered as a proper SCMs alternative in the construction industry due to its high pozzolanic reactivity and purity [22–24]. Several studies [25–27] reported that the application of high-reactivity MK in the cementitious composites led to better mechanical and durability properties. El-Diadamony et al. [28] observed that using 15 wt% MK in replacing cement improved the durability properties of lightweight-aggregate cementitious composites. Assem and Hassan [29] used up to 25 wt% MK as cement replacement, reporting that the chloride-ion penetration coefficient was reduced with increased MK dosage. Similarly, several studies [30–32] found that the addition of MK refined the microstructure of the MK-cement composites, improving its compressive strength and resistance against chloride-ion ingress. Cai et al. [33] explained that this phenomenon was attributed to the pozzolanic reactions between MK and the portlandite (CH) from the cement hydration, forming additional C-S-H and aluminate ferrite monosulfate (AFm) for a denser cementitious microstructure. In addition, Keleştemur and Demirel [34] stated that large surface are of MK offered more nucleation sites, promoting the hydration dynamics of MK-cement composites. Similarly, Papp et al. [35] observed that samples with up to 30 wt% MK exhibited total pore volume reduction when compared to the reference mix using Brunauer–Emmett–Telle (BET) analysis at 30 days, indicating the benefit of MK in refining the microstructure of MK-cement composites. In addition, Ulloa et al. [36] stated MK could be used in geopolymer-based composites, improving durability properties and self-healing capacities. However, due to cement dilution, the application of MK would lower the early strength of the MK-cement composites, highlighting a main weakness of AL-rich materials as the SCMs [37–39].

The synergistic effects of MK and other SCMs on further improving the properties of MK-cement composites were also studied [37,40], such as combination of MK and coral powder, MK and FA, and limestone (LS) and MK [38,41–43]. Qin et al. [42] used 10 wt% coral powder and up to 30 wt% MK as the cement replacement, found that hemicarboaluminate (Hc) or monocarboaluminate (Mc) formed to densify the cementitious matrix, leading to improved compressive strength. Sun et al. [44] used 30 wt% FA and up to 10 wt% MK as the cement replacement, reporting that samples with 30 wt% FA and 3 wt% MK had the highest compressive strength (35.9% increment) after 30 days of wet/dry cycle. They found that MK provided proper filler effect and high pozzolanic reactivity, densifying the cementitious microstructure. Antoni et al. [45] observed that the combination of 30 wt% MK and 15 wt% LS led to 14.3% and 17.7% strength increase for 7-day and 28-day compressive strength when compared to the reference mix. Tang et al. [46] observed that the synergistic effects of MK and LS was attributed to MK/LS ratio, while excessive dosage of MK or LS would lower the mechanical properties of the cementitious composites. Moreover, some studied [47,48] also found that the combination of MK and LS refined the cementitious matrix, leading to a denser microstructure. In addition, samples with the combination of MK and LS had better mechanical properties improvement than that of samples with the combination of FA and LS [49].

Although previous studies have explored the synergistic effects of MK and LS on the performance of cementitious composites, the understanding of their behavior under low water-to-binder (w/b) ratios, particularly in terms of early-age hydration kinetics, remains limited. In particular, quantitative insights into how MK–LS interactions influence phase assemblage, pore structure evolution, and early strength under low w/b conditions are lacking. The boundary nucleation and growth (BNG) model has been widely employed to simulate the hydration behavior of heterogeneous cementitious systems and supplementary cementitious material (SCM)-modified binders [50]. However, its application to MK–LS blended cement with a very low w/b ratio (≤0.16) has rarely been reported, and systematic analysis linking kinetic modeling to microstructural development is lacking. The coupling between hydration kinetics, the formation of carboaluminate phases (hemicarboaluminate and monocarboaluminate), and early-age strength gain in low w/b MK–LS-cement systems has not been clearly elucidated [51–54].

Therefore, this study aims to systematically investigate the early hydration kinetics, strength development, and microstructural evolution of MK-LS-cement composites with a low w/b ratio (0.16). The BNG model is employed to quantitatively analyse hydration kinetics, while X-ray diffraction (XRD), thermogravimetric analysis (TG/DTG), and pore structure characterization are used to elucidate phase assemblage evolution and microstructural refinement. This paper aimed to establish a mechanistic linkage between MK-LS synergistic reactions, hydration kinetics regulation, and early-age performance enhancement under low w/b conditions, thereby providing fundamental insights for the optimized design and practical application of low-carbon, sustainable cementitious composites. The significance of this study was to reveal the hydration and strength development of low w/b MK-LS-cement composites, expanding the application of MK and LS in the high-performance cementitious system.

2. Methodology

2.1. Raw materials and mortar fabrications

Commercially available P·I 52.5 Portland cement (Shandong Shanshui Cement Group, China), satisfying the requirements as per GB 175–2023 [55], was utilised as the main binder for casting mortar specimens. The density, specific gravity, and surface are of cement were 1430 kg/m^3, 1.801, and 354.3 m^2/kg respectively. Meanwhile, the C_3S, C_2S, C_3A, C_4AF, and lime saturation factor of this type of cement were 56.35, 22.41, 5.63, 2.24, and 0.82 respectively. MK and LS powder were obtained from Haofu Chemical Co., Ltd. (Shanghai, China). MK was grey powder (Fig. 1a), while LS was white powder (Fig. 1b). The particle size distribution (PSD) of all powders was analysed using a Microtrac laser particle size analyser (Fig. 1c). MK had the finest particle size (up to 10 μm) with a D50 value of 2.28 μm. The D50 value of LS and ordinary Portland cement (OPC) were 4.37 μm and 16.9 μm respectively. Based on a previous study [56], SCMs with different PSD could improve its filler effects in the cementitious matrix. The chemical compositions of all powders are shown in Table 1. MK contained large amounts of SiO_2 and Al_2O_3, being 52.9% and 42.8% respectively. Standard sand (Xiamen Ace Standard Sand Co., Ltd, China), satisfying sieving requirement as per GB 14684–2022 [57], was used as fine aggregate. The bulk density, fineness modulus, specific gravity, and water adsorption of this standard sand is 1580 kg/m^3, 2.7, 2.6, and 1.78% respectively.

Four mix designs were adopted to investigate the synergistic effects of MK and LS on the properties of the cementitious composites (Table 2). The water-binder-fine aggregate ratio was set as 0.16:1:1 for all groups. Approximately 4 wt% (by weight of total binder) Polycarboxylate superplasticiser (Jiangsu Subote Company, China) was used to improve the workability of samples with and without LS and MK. The superplasticiser is brown colour, and its specific gravity and pH value are 1.12 g/ml and 3.8 ± 0.1 respectively. C0 is the reference mix as the benchmark. Up to 20 wt% LS and 20 wt% MK were used to partially replace cement content by the weight of total binder, indicating C + LS and C + MK respectively. In C + LSMK group, a LS/MK ratio of 1:2 was adopted, and the total cement replacing dosage was 20 wt%. As a result, the effects of LS, MK, and combination of LS and MK on the early hydration and strength development of the mortar samples could be compared. It should be noted that the flow test was carried out in accordance with GB 8077–2023 [58] and the flow result of each group was summarised in Table 2.

Firstly, dry binders were pre-mixed using a 5-L Hobart Mixer at 16 rpm for 2 mins allowing a uniform powder mixture, and the

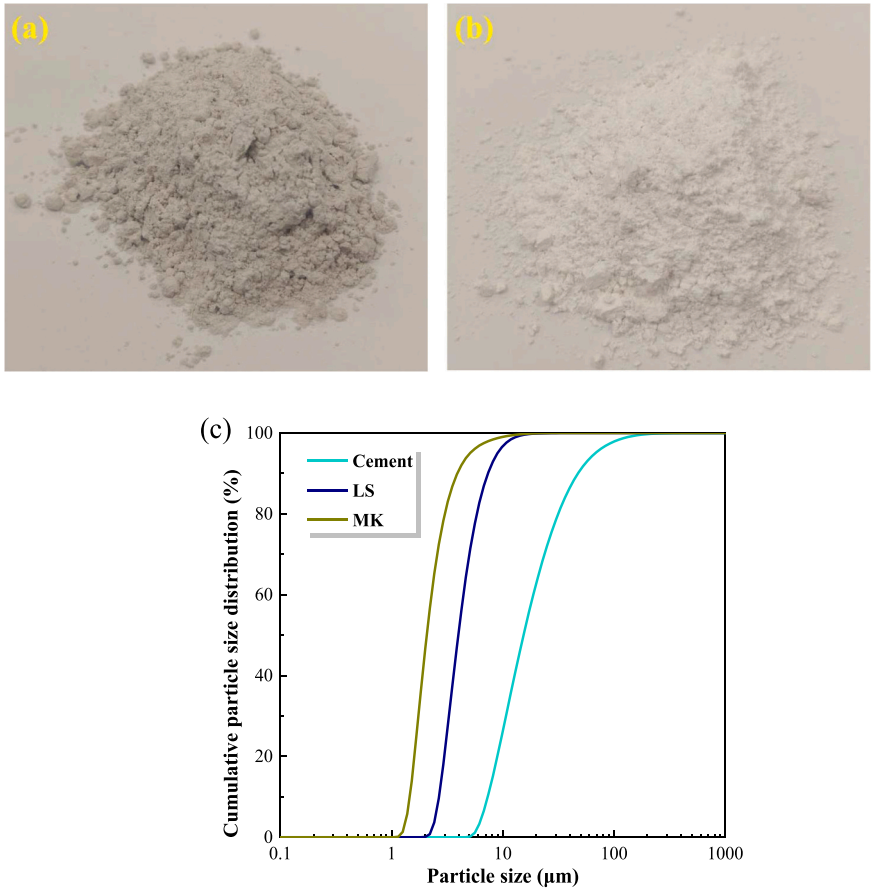

Fig. 1. Raw materials: (a) MK; (b) LS; (c) Binder particle size distribution.

Table 1
XRF results.

Chemical compositions	OPC	LS	MK
SiO_2	23.7	3.52	52.9
CaO	61.2	90.9	0.26
Al_2O_3	5.9	0.51	42.8
SO_3	2.36	0.05	0.02
Na_2O	0.32	0.1	0.1
MgO	0.65	2.78	0.84
K_2O	0.64	0.07	0.12
Fe_2O_3	2.1	0.32	0.51
L.O.I.	1.38	0.18	1.68

Table 2
Mix Proportions of the Mortars Used (in ratio).

Mix designs	OPC	LS	MK	Water	Sand	PCE	w/b ratio	Flow (mm)
C0	1	-	-	0.16	1	0.04	0.16	168 ± 2.2
C + LS	0.8	0.2	-	0.16	1	0.04	0.16	166 ± 2.4
C + MK	0.8	-	0.2	0.16	1	0.04	0.16	165 ± 1.2
C + LSMK	0.8	0.066	0.134	0.16	1	0.04	0.16	163 ± 1.9

Note: OPC means ordinary Portland cement, and PCE means Polycarboxylate superplasticizer

powder mixture was then stored in a dry container. Dry sand was mixed with 1/2 water content for 1 min. After that, the pre-mixed powder and the rest of water were added following another 3-min medium mixing at 24 rpm. Fresh cementitious mixture was then poured into $50mm \times 50mm \times 50mm$ and $40mm \times 40mm \times 160mm$ moulds respectively, following a 2-min vibration for a uniform compaction. It should be noted that plastic foil was used to cover all moulds till 24-hour demoulding. Finally, samples were stored in a conditioned chamber with 23 ± 2 °C temperature and 95 ± 5% relative humidity until formal mechanical testings.

2.2. Hydration kinetics

Approximately 10 g of fresh paste was casted for each group using the sample mix design listed in Table 2. An 8-channel TAM air isothermal calorimetry (Thermometric AB, USA) was used to record the hydration evolution of all groups as per ASTM C1702–17. The reference temperature of 20 °C was adopted, and the hydration development of all groups were recorded up to 96 h.

2.3. Mechanical properties

Mortar cubes and prisms were removed from the conditioned chamber after 3-day exposure. The 3-day compressive strength and flexural strength were tested using a UH500 universal machine and an AGX50 testing machine respectively as per GB 17671–2021. It should be mentioned that the 3-day mechanical properties of each group were the average of three identical testing results.

2.4. Microstructural analysis

Additional fresh paste samples were prepared for all groups according to the mix design in Table 2. It is worth noting that 1-day and 3-day paste pieces were collected and stored in an isopropanol solution with 99% purity for 7 days to stop hydration. After that, all paste pieces were dried in an oven at 40°C for 7 days. A ring mill was used to ground all samples to pass a 100-μm sieve.

XRD analysis of 1-day and 3-day samples was conducted using a Rigaku D/Max-RB X-ray diffractometer (Cu Kα, $\lambda = 1.54$ Å), with a scanning range of 5° to 60° 2θ at a scanning rate of 10°/min. The phase assemblage of each group was analysed using Crystallography Open Database.

TG analysis was performed using a TGA equipment (TA, Naichi). The heating range was set up to 1000°C at a heating rate of 10°C/min in a N_2-environment chamber. The N_2 flow was set at 50 ml/min for all TG analysis. After that, TG and DTG results were used to analyse the hydration products of all groups after 3-day exposure.

An Autosorb-iQ3 instrument (Quantachrome, USA) was utilised to measure the nitrogen adsorption/desorption of all groups after 3-day exposure. It should be noted that all powders were further dehydrated at 200°C for 2 h, removing water and gas impurities. The pore distribution of all groups was obtained from the adsorption/desorption curve in the range of 1 nm to 200 nm.

3. Results

3.1. Hydration evolution

The hydration kinetics per unit binder of all groups are depicted in Fig. 2, including normalised heat (Fig. 2a) and normalised heat

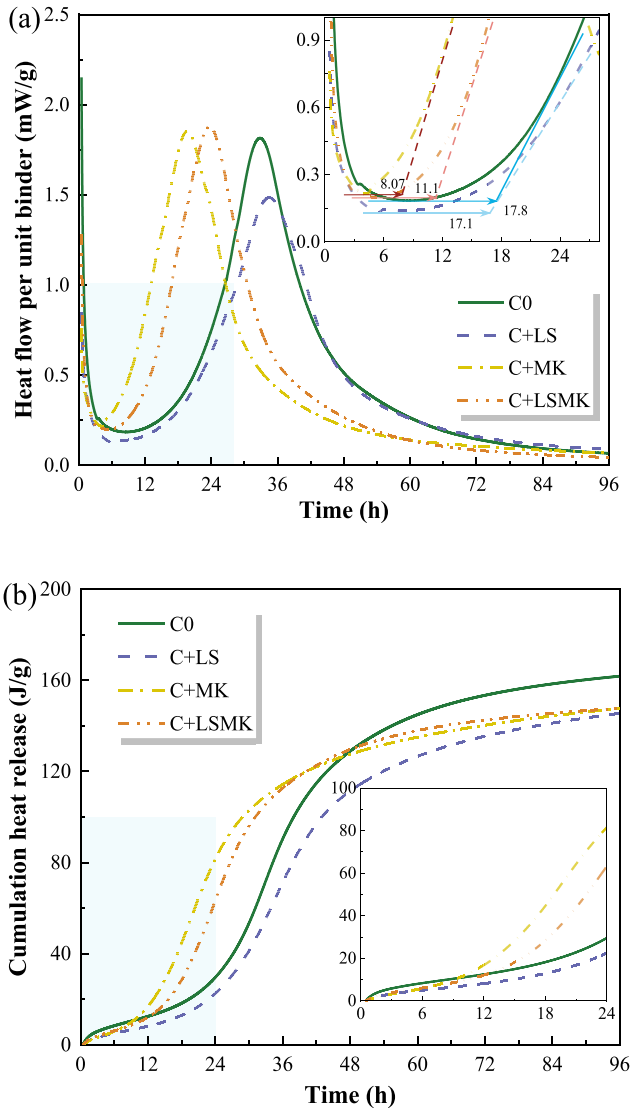

Fig. 2. Hydration kinetics of all mortars per unit binder: (a) Normalised heat to heat flow; (b) Normalised heat to cumulative heat release.

(Fig. 2b). Normally, the hydration development of cementitious system could be divided into four stages: initial stage, induction stage, acceleration stage, and deceleration stage [50]. There were two key points in the cement hydration evolution: (1) transition point 1 ($t_{i\rightarrow a}$) from the induction stage to the acceleration stage; (2) transition point 2 ($t_{a\rightarrow d}$) from the acceleration stage to the deceleration stage. However, considering the difficulty in exactly determining the two turning points, this study adopted that the transition point ($t_{i\rightarrow a}$) was the X-axis coordinate value of the point, being the intersection point of the tangent line at the minimum value of the induction stage and the tangent line at the turning point of the acceleration stage (Fig. 2a) as per a previous study by Long et al. [50]. This tangent-based approach was selected as it provided a reproducible approximation of the onset of acceleration when direct visual

Table 3
Characteristic parameters of hydration kinetics of all groups.

Mix designs	Transition point $t_{i\rightarrow a}$		Transition point $t_{a\rightarrow d}$		1-day cumulative heat (J/g)	3-day cumulative heat (J/g)
	Time (h)	Heat flow (mW/g)	Time (h)	Heat flow (mW/g)		
C0	17.8	0.34	32.7	1.81	29.6	153.4
C + LS	17.1	0.27	34.3	1.48	22.5	135.4
C + MK	8.07	0.40	19.7	1.85	81.6	140.3
C + LSMK	11.1	0.36	23.7	1.88	63.3	142.6

identification was ambiguous. Then, the transition point ($t_{a\rightarrow d}$) was the X-axis coordinate value of another point, being the peak point of the normalized heat flow per unit binder curve (Fig. 2a).

The parameters of each hydration kinetics curve are summarised in Table 3. Due to the presence of 4 wt% PCE, the induction period and hydration peaks of all groups with low w/b ratio of 0.16 were delayed significantly when compared to those of cement paste with normal w/b ratio of 0.4–0.5, having a good agreement with a previous study [59]. The heat flow peak of C + LS group was lower than that of the reference mix. Advanced time points of the heat flow peak were observed for C + MK and C + LSMK group, while remaining similar values of heat flow peak when compared to the reference mix. As shown in Table 3, the value of $t_{i\rightarrow a}$ and $t_{a\rightarrow d}$ of the reference mix was 17.8 h and 32.7 h respectively. However, the value of $t_{a\rightarrow d}$ of C + LS was delayed to 34.3 h with a heat flow reduction (18.2%) when compared to C0 group. This fact may be attributed to the low reactivity of LS providing limited improvement in cement hydration. The value of $t_{i\rightarrow a}$ and $t_{a\rightarrow d}$ of the C + MK group was advanced to 8.07 h and 19.7 h respectively. The heat flow of C + MK at $t_{a\rightarrow d}$ was similar to that of the reference mix. In terms of samples with LS and MK addition, the heat flow trend was similar to that of C + MK group, also having a similar heat flow peak ($t_{a\rightarrow d}$) with the reference mix. In addition, the 1-day cumulative heat per unit binder of C + MK and C + LSMK was significantly higher than that of C0 group. However, the 3-day cumulative heat per unit binder of C + MK and C + LSMK was slightly lower than that of the reference mix (Table 3).

Fig. 3 presents the hydration kinetics per unit cement for all groups. The heat flow peak per unit cement of C + MK and C + LSMK group was higher than that of the reference mix, while C + LS had similar heat flow peak with the reference mix (Fig. 3a). Samples with different SCMs had higher cumulative heat per unit cement than C0 after 3 days (Fig. 3b). Specifically, when compared to the reference mix, the 1-day and 3-day cumulative heat per unit cement of C + MK group was improved by 245% and 14.3% respectively. Similarly,

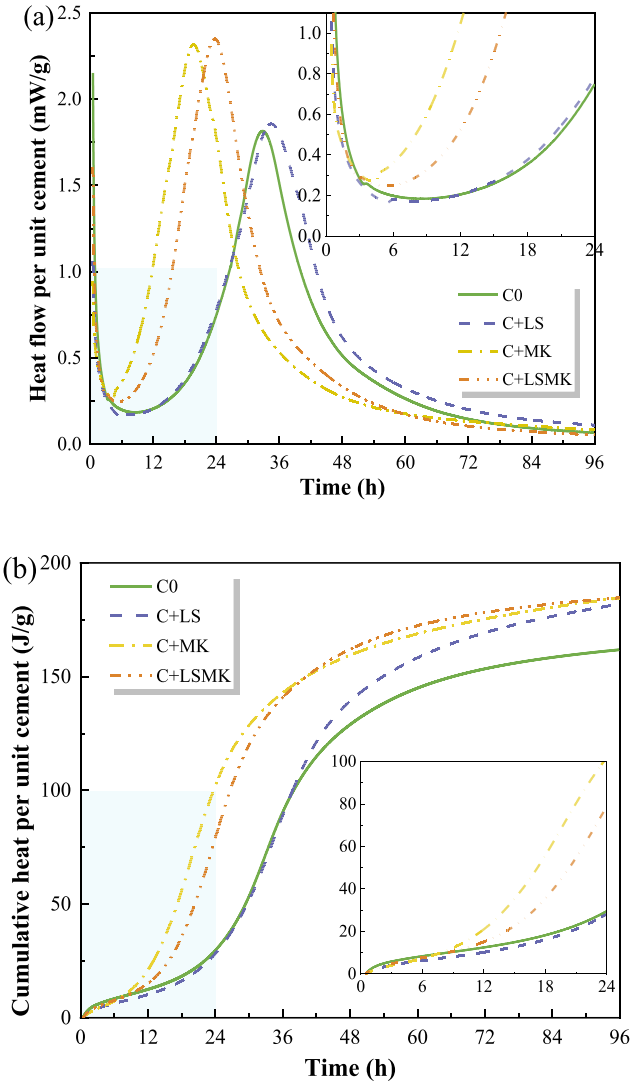

Fig. 3. Hydration kinetics of all mortars per unit cement: (a) Normalised heat flow; (b) Normalised heat.

the 1-day and 3-day cumulative heat per unit cement of C + LSMK group was improved by 167% and 16.2% respectively. Noticeably, the cumulative heat per unit cement of C + LSMK was higher than that of C + MK group after 2 days. This was attributed to possible pozzolanic reactions between MK, LS and CH, releasing additional heat. One interpretation might be that the pozzolanic reactions did not occur immediately during the early hydration. However, the activation of pozzolanic reactions contributed to additional heat generation, compensating more heat generation for the presence of limestone without reactivity. As a result, the heat development of C + LSMK was slightly higher than that of C + MK.

3.2. Mechanical properties

Fig. 4 shows the 3-day mechanical properties of all groups. It should be noted that the mechanical properties were calculated based on three identical testings of each group. The 3-day compressive strength of the reference mix was 63 MPa as the benchmark. The 3-day compressive strength of C + LS and C + MK group was reduced by 17.5% and 9.5% respectively when compared the reference mix (Fig. 4a). However, C + LSMK group had a similar 3-day compressive strength than that of C0 group. Apparently, the combination of MK and LS led to a better strength development when compared to C + LS and C + MK group. One interpretation was that although all three group experienced cement dilution, the activation of pozzolanic reactions compensate the additional formation of hydration products, leading to a denser microstructure for load-bearing capacity.

According to Fig. 4b, when compared to samples with only 20 wt% LS or MK, C + LSMK group exhibited a higher 3-day flexural strength. This was attributed to the synergistic effect of LS and MK improving the cement hydration, being in a good agreement with a previous study [60]. However, due to the cement dilution effect, the 3-day flexural strength of C + LSMK was reduced by 3.3% when compared to C0 group.

Overall, the results in mechanical testings had a good agreement with hydration development (Fig. 3). Comparing the strengths of mortar specimens with SCMs, C + LSMK had the highest heat release at 3 days, where additional pozzolanic reactions would lead to a denser microstructure when compared to C + LS or C + MK group. As a result, C + LSMK exhibited the highest 3-day mechanical strengths among three groups, being comparable to those of the reference mix.

3.3. Phase assemblage

Fig. 5 depicts the 1-day and 3-day XRD patterns for all groups. The main phases in the paste samples included cement clinker (CS: alite and belite), CH, ettringite, and calcite (CC). The CH diffraction peaks of C + MK and C + LSMK were lower than those of the reference mix at 3 days (Fig. 5b), being attributed to the pozzolanic reactions consuming a portion of CH. Significant diffraction peaks of CC were found in C + LS and C + LSMK samples. This phenomenon was due to the presence of LS as the filler effect in the cementitious matrix. In addition, the diffraction peaks of 12.5° 2θ and 13.3° 2θ indicated the formations of Hc and Mc, being consistent with a previous study [61]. It should be noted that C + LSMK group exhibited the highest peaks of Hc and Mc, highlighting the synergistic effects of MK and LS promoting the formation of these aluminium-based phases. Higher content of hemicarboaluminate (Hc) or monocarboaluminate (Mc) could improve C + LSMK samples' resistance against chloride ingress, due to refined microstructure and higher chloride-binding capacity [62,63]. Some studies [63,64] reported that the formation of Hc or Mc filler in pores in the cementitious matrix, limited the access of chloride ions to deeper matrix. Meanwhile, formation of Hc and Mc could chemically bind chloride ions, improving the performance of chloride stability.

The TG/DTG results of all paste samples after 3-day exposure are given in Fig. 6. According to DTG curve (Fig. 6a), the first endothermic peak in the temperature range of 50–300°C was due to the mass loss of physical and chemical bound water in the hydration products [65]. In particular, the mass loss of chemical bound water was mainly located in temperature range of 105–300°C. The second endothermic event (300–400°C) was attributed to the dehydration of PCE [66]. Furthermore, the third and fourth endothermic peak could be interpreted as the decomposition of CH (400–500°C) [67] and the decarbonation of CC (500–800°C) respectively [68].

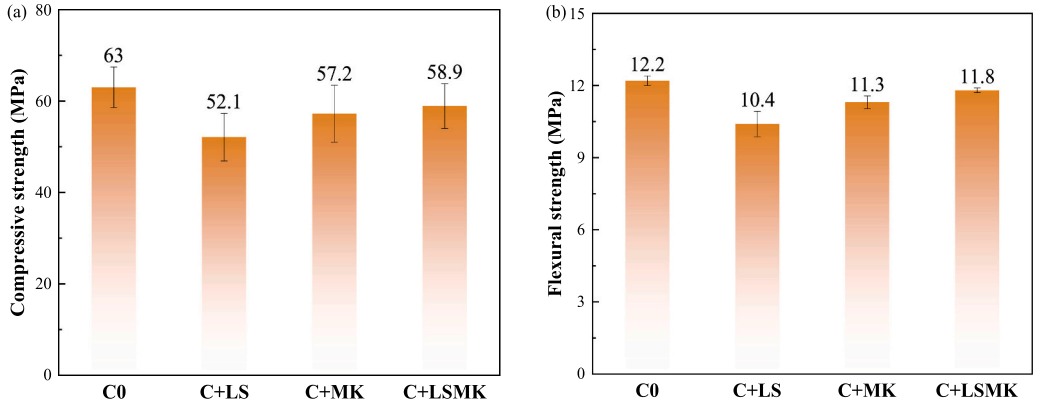

Fig. 4. 3-day mechanical properties: (a) Compressive strength; (b) Flexural strength.

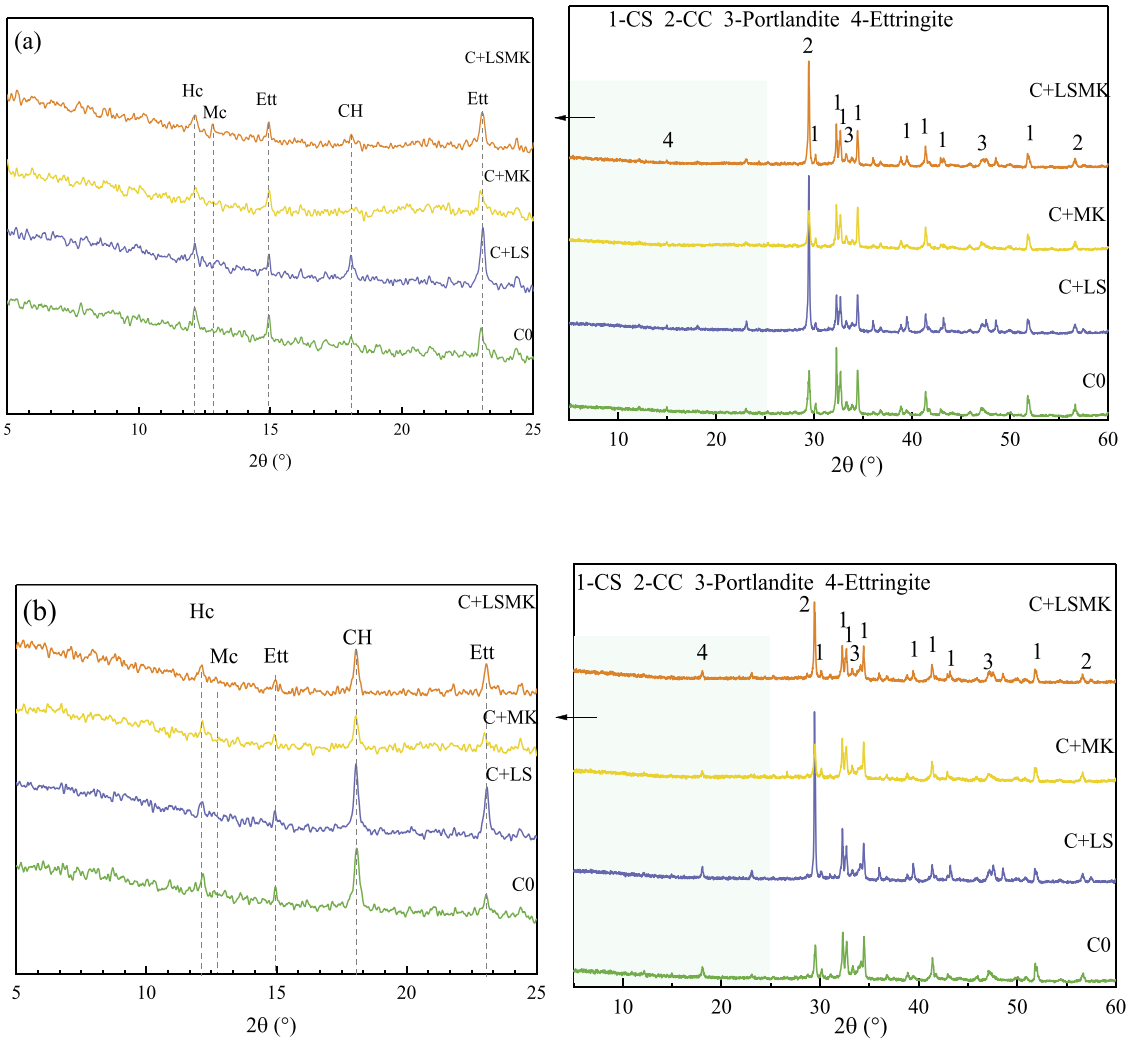

Fig. 5. XRD patterns: (a) 1-day exposure; (b) 3-day exposure, (Note: CS = cement clinker (alite and belite); CC = calcite; Ett = ettringite;.

The mass loss of chemical bound water (*mCBW*), CH (*mCH*), and CC (*mCC*) could be estimated using Eqs. (1–3) [69]:

$$mCBW = [(M105 - M300) + (M400 - M500)] \times 100\% \quad (1)$$

$$mCH = (M400 - M500) \times \frac{74}{18} \times 100\% \quad (2)$$

$$mCC = (M500 - M800) \times \frac{100}{44} \times 100\% \quad (3)$$

where M_{105}, M_{300}, M_{400}, M_{500}, and M_{800} means the mass loss percentage in the corresponding temperature in TG results. The numbers of 18, 44, 74, and 100 refer to the molar mass of water, carbon dioxide, CH, and calcite respectively.

The mass loss percentage of chemical bound water and CH and CC is shown in Fig. 6c and Fig. 6d respectively. Due to the cement dilution effect, samples with SCMs had lower mass loss of chemical bound water than the reference mix (Fig. 6c). The C0 group exhibited the highest *mCBW* value of 3.87%, while C + MK had the lowest *mCBW* value of 3.59%. In terms of samples with SCMs, C + LSMK group exhibited the highest *mCBW* value among three groups, indicating additional formation of hydration products. As shown in Fig. 6d, the CH contents of C + MK and C + LSMK were lower than that of the reference mix. This phenomenon was due to the CH consumption in the pozzolanic reactions, being consistent with observations in XRD patterns (Fig. 5b). Furthermore, due to the presence of LS in C + LS and C + LSMK paste samples, significant mass loss of CC was observed in these two groups.

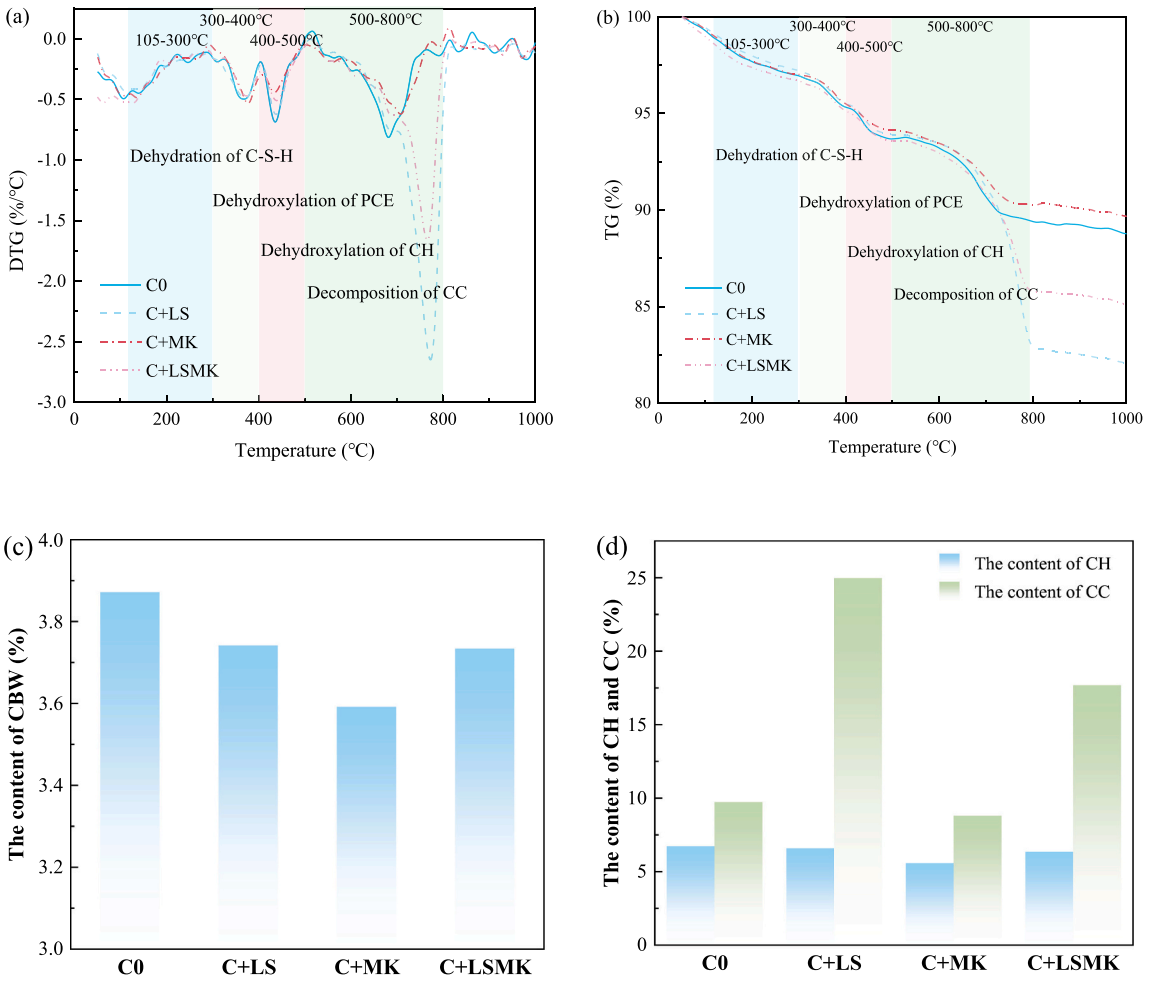

Fig. 6. TG/DTG analysis at 3 days: (a) DTG curve; (b) TG curve; (c) Mass loss of chemical bound water; (d) Mass loss of CH and CC.

3.4. Pore structure analysis

Fig. 7 shows the pore structure of paste samples at 3 days. Based on available literatures, gel pores had pore diameters below 10 nm, while the pore diameters of capillary pore were higher than 10 nm [70,71]. Based on Fig. 7a, C + LS group had the lowest N_2 adsorption/desorption values, while C + LSMK had the highest N_2 adsorption/desorption values. Using Barett-Jonyer- Halenda (BJH) method to analyse the pore diameters (Table 4), the apparent surface area (ASA) of C0 group was 6.384 m^2/g with most probable pore diameter of 32.6 nm as the benchmark. When using 20 wt% LS as cement replacement, the apparent surface area was reduced to 4.902 m^2/g, while samples with 20 wt% MK only remained a similar ASA value than the reference mix. However, using LS and MK as the combination to replace 20 wt% cement, the ASA was improved by 16.6%. Meanwhile, the most probable pore diameter in C + LSMK group was reduced to 28.9 nm (11.35% reduction), while remaining a similar total pore volume with the reference mix (Table 4). This result could be interpreted as that due to pozzolanic reactions in C + LSMK group, the formation of Hc or Mc refined the pore structures of the microstructure of the C + LSMK group, leading to the size reduction of the most-portable pores. This reduction reflected a denser microstructure in C + LSMK when compared to the reference mix.

4. Discussions

4.1. Hydration dynamic modelling

The results from isothermal calorimetry could be used to determine the rate of hydration heat release (dQ/dt) and the relationship between hydration heat (Q) and time (t) for all groups. The hydration degree α(t) at time t could be estimated using Eqs. (4–6) [66,69]:

$$\alpha(t) = \frac{Q(t)}{Q_{max}} \tag{4}$$

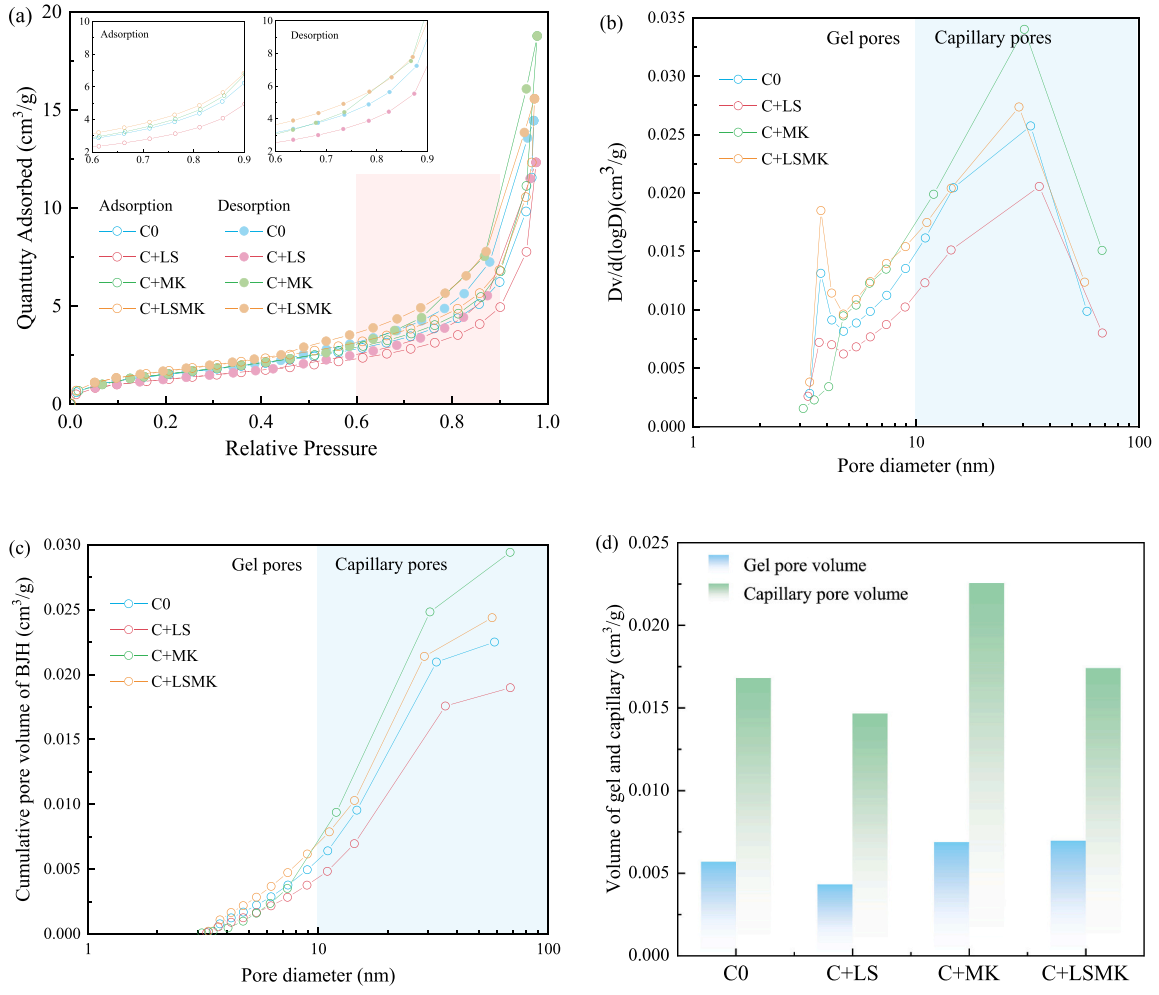

Fig. 7. Pore structure of all groups: (a) Nitrogen adsorption/desorption curve; (b) Pore distribution; (c) Cumulative pore volume; (d) Volume of gel and capillary pore.

Table 4
Pore structure parameters of all groups.

Mix design	ASA, m^2/g	Pore Volume, cm^3/g	Most probable pore size, nm
C0	6.384	0.02250	32.6
C + LS	4.902	0.01898	35.7
C + MK	6.761	0.02942	30.6
C + LSMK	7.442	0.02438	28.9

$$\frac{d\alpha}{dt} = \frac{dQ}{dt} \bullet \frac{1}{Q_{max}} \tag{5}$$

$$\frac{1}{Q} = \frac{1}{Q_{max}} + \frac{t_{50}}{Q_{max}(t - t_0)} \tag{6}$$

where Q_{max} is the total heat of a cementing system; t_0 refers to the time that induction stage ends; and t_{50} is the time when 50% of total heat Q_{max} is reached.

The Q_{max} and the degree of hydration $\alpha(t)$ of all paste groups are presented in Fig. 8. C + LS group exhibited the lowest hydration degree at 24 h among all groups, being 19.7% lower than that of the reference mix (Fig. 8b). However, the degree of hydration of C + MK and C + LSMK reached 0.47 and 0.39 respectively, being 279.1% and 214.5% higher than that of C0 at 24 h. At 72 h, 20 wt% LS led to 7% reduction in the hydration degree when compared to the reference mix. Furthermore, C + LSMK group exhibited the

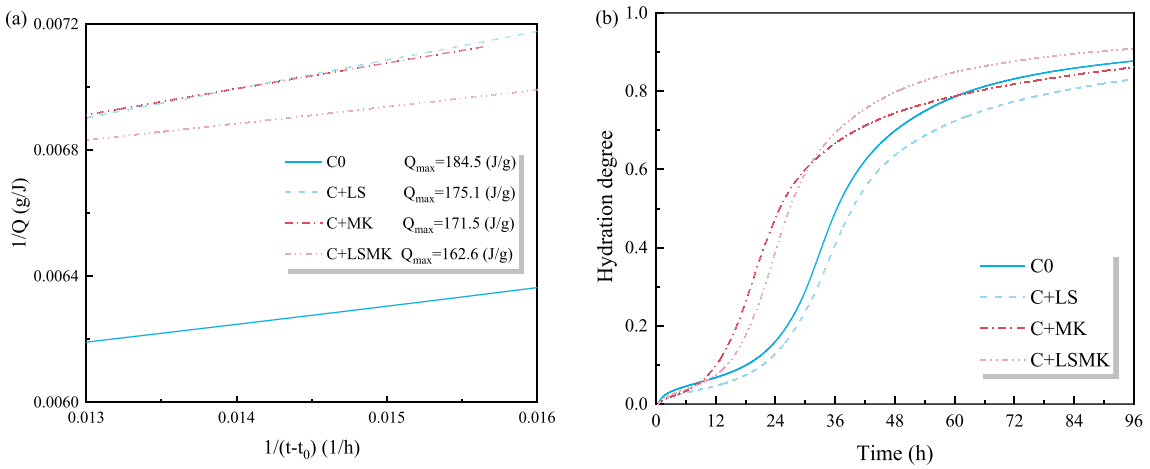

Fig. 8. Hydration development of all groups: (a) Linear fitting result of Q_{max}; (b) Hydration degree;.

highest 72-hour hydration degree among samples with SCMs, being slightly higher than the reference mix.

To quantitatively analyse the nucleation and growth rate of the paste samples, Thomas [72] proposed BNG model for the tricalcium silicate (C_3S) hydration. When comparing to the Krstulovic-Dabic model and the JMAK model [73], the primary advantage of BNG model was that it considered C-S-H gel only formed on the surface of the C_3S grains, which could be expressed as Eq. 7 [74,75]:

$$V = 1 - \exp\{-2pSGt \int_0^1 (1 - \exp\left[-\frac{\pi N}{3} gG^2 t^3 (1-u)^2 (1+2u)\right])\} \tag{7}$$

where V is the volume fraction of cement grains at time t; t is the hydration time; u refers to a variable related to growth rate; p is the ratio of external growth rate and internal growth rate of the cement grain, if we assume two growth rates is the same, $p = 1$; S means nucleation surface are per unit volume, set $S = 1.1448\ \mu m^{-1}$; g is the coefficient of the growth rate in the tangential direction, if we assume the growth rate is isotropic, $g = 1$; N and G are the nucleation rate and the growth rate of crystals in the normal direction. In addition, we define:

$$k_G = pSG\ ,\ k_N = \frac{\pi N g G^2}{3} \tag{8}$$

Thus, Eq. 7 could be rearranged as:

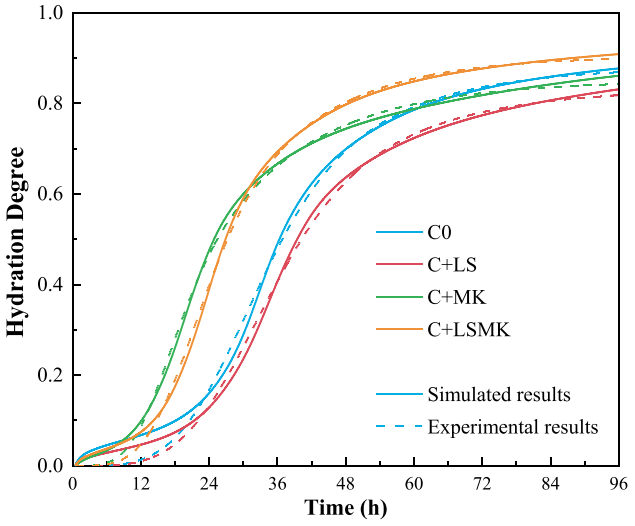

Fig. 9. Fitting curves of hydration degree of all groups using BNG model.

$$V = 1 - \quad \exp\{-2k_G t \int_0^1 \left[1 - \exp\left[-k_N t^3 (1-u)^2 (1+2u)\right]\right]\} \tag{9}$$

It should be noted that there is a linear relationship between the volume fraction V and cumulative hydration heat $Q(t)$, that is:

$$V = A \bullet Q(t) \tag{10}$$

$$V = A \bullet \alpha(t) \bullet Q_{max} = A' \bullet \alpha(t) \tag{11}$$

where A and A' are the proportional factor coefficients.

Fig. 9 shows the fitting curves of hydration degree of all paste samples, and the kinetic parameters of BNG model are summarised in Table 5. Based on BNG model, the degree of hydration of all groups were simulated properly, indicating that BNG model could be effectively used to estimate the hydration development of sample with both LS and MK. The values of R^2 are higher than 0.99 for all groups (Table 5). It is worth mentioning that the *N* of samples with low w/b ratio was lower than that of samples with normal w/b ratio of 0.4–0.5 [76,77]. C + MK group exhibited the highest nucleation rate *N* (0.484), followed by C + LSMK (0.173), while C + LS had a similar *N* value with the reference mix. This phenomenon revealed that finer-size MK particles with high apparent surface area led to better nucleation effects in the early hydration of the cementitious composites. In terms of growth rate *G*, C + LS group had the lowest growth rate, indicating slow early hydration development. However, C + LSMK sample displayed the highest hydration growth rate. This result indicated that more hydration products were formed in C + LSMK sample, having a good agreement with TG/DTG results.

4.2. Synergistic effects of MK and LS

To date, many studies have been conducted to explore the effects of LS or MK as cement replacement on the cementitious composites [78]. The addition of LS could provide proper filler effects and a portion of LS could react with calcium aluminate to form Hc, refining the pore structure and densifying the cementitious microstructure [79]. However, due to low reactivity of LS powder and low aluminium phases in OPC, only limited hydration improvement could be found in LS-cement composites. This mechanism could be used to explain low hydration heat in C + LS groups (Fig. 2 and Fig. 3), leading to lower mechanical properties in C + LS mortar samples (Fig. 4). However, when using the combination of MK and LS to replace 20 wt% cement content, MK powder provided more portion of soluble silica and alumina (AS_2), while LS provided more CO_3^{2-} in the pore solution at the early hydration. As a result, AS_2 promoted the formation of hemicarboaluminate, which gradually converted into monocarboaluminate in the later hydration (Fig. 5). This reaction could be expressed as Eq. 12 [80]:

$$AS_2 + CC + Ca(OH)_2 + H_2O \rightarrow CAC_nH \tag{12}$$

where AS_2 refers to silica and alumina in MK; CC means calcite in LS; CAC_nH is calcium carbonate aluminate, e.g. n = 0.5 for Hc, and n = 1 for Mc.

Fig. 10 depicts the synergistic effects of MK and LS in the cementing system. It should be noted that the formation of Mc refined the pore structure densifying the cementitious matrix, contributing to a denser microstructure. In addition, high apparent surface area of MK could promote the nucleation effects, while high portion of silica and alumina promoting the pozzolanic reactions [81]. Hence, the hydration kinetics of C + LSMK group were improved (Fig. 9 and Table 4), forming more hydration products (Fig. 6). Meanwhile, C + LSMK group also exhibited a higher volume of capillary pore and lower cumulative pore volume. Thus, it could be safely concluded that the synergistic effects of MK and LS was attributed to the reaction between AS_2, CC, and CH [82], leading to higher mechanical properties of C + LSMK group (Fig. 4).

5. Conclusion

This study investigated the early hydration process, strength development, and microstructure evolution of MK-LS-cement composites with low w/b ratio of 0.16. Meanwhile, BNG model were used to analyse the hydration development of all groups. The main conclusions were drawn as the follows:

1) The addition of MK led to early heat flow peak of the MK-cement composites, remaining similar hydration heat when compared to MK-free samples. Samples with 20 wt% LS had the lowest hydration heat.
2) Samples with C + LSMK remained comparable 3-day mechanical strength with the reference mix. Using 20 wt% LS as cement replacement (C+LS) led to 17.5% reduction in 3-day compressive strength when compared to the reference mix, being attributed to low reactivity of LS powder and cement dilution.
3) XRD patterns revealed higher intensity of Hc and Mc in C + LSMK group. TG/DTG further confirmed CH was consumed to form Hc or Mc.
4) Using Barett-Jonyer-Halenda (BJH) method, C + LSMK group exhibited reduced pore sizes than the reference mix, indicating more formation of hydration products (e.g. C-S-H gels) promoting the early strength development.
5) Based on BNG model, C + LSMK group exhibited improved cement hydration, being attributed to finer-size MK particle as fillers and induction of pozzolanic reactions.

Table 5
Hydration kinetic parameters in BNG model.

Mix designs	k_G	k_N	N ($\mu m^{-2} \cdot h^{-1}$)	G ($\mu m \cdot h^{-1}$)	R^2
C0	0.0246	3.01×10^{-5}	0.062	0.0215	0.9955
C + LS	0.0233	2.54×10^{-5}	0.059	0.0203	0.9973
C + MK	0.0250	2.42×10^{-4}	0.484	0.0218	0.9983
C + LSMK	0.0272	1.02×10^{-4}	0.173	0.0237	0.9984

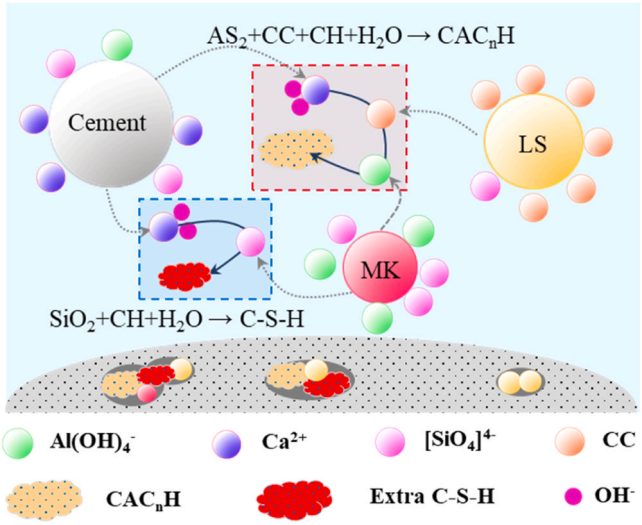

Fig. 10. Synergistic effects of MK and LS in the cementitious composite.

6) The synergistic effect of MK and LS promoted the reactions between MK powder, calcite and CH, forming Hc or Mc to refine the cementitious matrix.

Overall, the combination of MK and LS as cement replacement provided favourable improvement in the cementitious matrix with refined microstructure. It is encouraged that more studies are needed to further analyse the optimum dosage of MK and LS enhancing both mechanical and durability resilience of the cementitious composites.

CRediT authorship contribution statement

Xuan Sun: Software. **Dongdong Wang:** Investigation. **Peimin Zhan:** Writing – original draft, Visualization, Conceptualization. **Xuqun Lin:** Writing – review & editing, Visualization. **Juan Wang:** Writing – review & editing, Funding acquisition. **Dapeng Wang:** Software, Resources. **Weiwei Lin:** Validation. ***, Vivian W. Y.:** Validation, Supervision.

Declaration of Competing Interest

The authors declare that they have no known competing financial interests or personal relationships that could have appeared to influence the work reported in this paper.

Acknowledgement

The authors highly appreciate Australian Research Council, Australia (DP220101051) and the supports from University of Technology Sydney Research Academic Program at Tech Lab (UTS RAPT), as well as the support by Shanghai Pujiang Programme (24PJB033).

Data availability

Data will be made available on request.

References

[1] J. Miao, S. Xiao, Y. Zhou, W. Chen, Y. Jin, L. Cheng, C. Chang, H. Zhang, Biochar-zeolite modified super sulphate cement as a high-performance, sustainable and high-efficiency CO_2 sequestration cementitious material, Constr. Build. Mater. 490 (2025) 142475.
[2] P. Ye, B. Guo, H. Qin, C. Wang, J. Li, Y. Chen, D. Lu, L. Wang, P. Gao, P. Ma, B. Zhan, Q. Yu, Investigation of the properties and sustainability of modified biochar-doped cement-based composite, Cem. Concr. Compos. 153 (2024) 105684.
[3] A. Dixit, H. Du, S.D. Pang, Carbon capture in ultra-high performance concrete using pressurized CO2 curing, Constr. Build. Mater. 288 (2021) 123076.
[4] X. Lin, W. Li, Y. Guo, W. Dong, A. Castel, K. Wang, Biochar-cement concrete toward decarbonisation and sustainability for construction: characteristic, performance and perspective, J. Clean. Prod. 419 (2023) 138219.
[5] T. Wu, S.T. Ng, J. Chen, Deciphering the CO2 emissions and emission intensity of cement sector in China through decomposition analysis, J. Clean. Prod. 352 (2022) 131627.
[6] W. Li, Y. Liu, H. Li, X. Yu, P. Zhu, Rheological properties of fresh limestone-metakaolin-cement system, Bull. Chin. Ceram. Soc. 42 (02) (2023) 411–419.
[7] Z. Zhang, S. Luo, X. Lin, Anisotropic of 3D printed cement-based materials reinforced with metakaolin and limestone powder, Bull. Chin. Ceram. Soc. 43 (05) (2024) 1651–1662. +1682.
[8] X. Li, A. Wanner, C. Hesse, S. Friesen, J. Dengler, Clinker-free cement based on calcined clay, slag, portlandite, anhydrite, and C-S-H seeding: An SCM-based low-carbon cementitious binder approach, Constr. Build. Mater. 442 (2024) 137546.
[9] Y. Zhang, X. Zhang, Z. Lu, K. Wu, X. Cai, New insight into the effects of silane-modified silica fume on the performance of cement pastes, Cem. Concr. Res. 190 (2025) 107818.
[10] J. Liu, L. Wu, J. Zhu, H. Jia, L. Liu, S. Zhang, C. Yang, Z. Chen, C. Shi, Effect of silica fume on corrosion resistance of cement-based materials under carbonic acid water environment, Cem. Concr. Compos. 157 (2025) 105949.
[11] S. Yang, X. Dong, X. Zhao, J.-X. Lu, H. Cui, C.S. Poon, High value-added utilization of waste glass powder and steel slag for a novel zero-clinker cement: coactivation mechanism and environmental impact, Constr. Build. Mater. 474 (2025) 141032.
[12] F. Zhou, G. Pan, Q. Wang, S. Li, J. Zhang, H. Sun, I. Saqib, Effects of the surface nano-reconstruction of steel slag on the performance of cement-based materials, Constr. Build. Mater. 475 (2025) 141172.
[13] A. Trisna Yudhistira, A. Nugroho, I. Satyarno, T. Handayani, M. Sandanayake, R. Erlangga, J. Lianto, A. Ernanto, Optimizing concrete mix design for cost and carbon reduction using machine learning, J. Human. Earth Future 6 (2025) 293–310.
[14] M. Irshidat, H. Kailani, Sustainable utilization of recycled concrete powder as sand replacement in cement mortar production: impact of sand-cement ratio, Civil. Eng. J. (2025).
[15] D. Lee, W.K. Kim, J. Moon, Enhanced carbonation performance of rice husk ash blended cement-based composites through in-situ CO2 mixing, Cem. Concr. Compos. 160 (2025) 106040.
[16] Y. Guo, J. Zhang, M.T. Lakhiar, J. Wang, Eco-friendly cement mortar production using rice husk ash and oyster seashell powder: a comprehensive study of mechanical, durability and life cycle properties, Constr. Build. Mater. 481 (2025) 141590.
[17] B. Zhang, H. Tan, W. Shen, G. Xu, B. Ma, X. Ji, Nano-silica and silica fume modified cement mortar used as Surface Protection Material to enhance the impermeability, Cem. Concr. Compos. 92 (2018) 7–17.
[18] X. Sun, J. Liu, Y. Zhao, J. Zhao, Z. Li, Y. Sun, J. Qiu, P. Zheng, Mechanical activation of steel slag to prepare supplementary cementitious materials: a comparative research based on the particle size distribution, hydration, toxicity assessment and carbon dioxide emission, J. Build. Eng. 60 (2022) 105200.
[19] R. He, J. Guo, Z. Wei, W. Li, Influence of rice husk ash and super-absorbent polymer on the properties of cement-based composites, Constr. Build. Mater. 450 (2024) 138623.
[20] K.M. Khedher, Experimental Behavior of Self Compacting Concrete Using Red Mud, Mesop. J. Civil. Eng. 2023 (2023) 10–17.
[21] A.M. Hamad, H.M. Issa, R.A. Salih, J. Keighobadi, A.B. Alias, R.A. Hasan, N.M. Saleh, A.M. Ali Mohammed Saleh, H.M. Hamada, I.I. Ghdhban, A Review on the Impact of Fly Ash on the Resistance of Ultra-High Performance Concrete to Acid and Sulfate Attacks, ESTIDAMAA 2024 (2024) 7–14.
[22] C. He, B. Osbaeck, E. Makovicky, Pozzolanic reactions of six principal clay minerals: Activation, reactivity assessments and technological effects, Cem. Concr. Res. 25 (8) (1995) 1691–1702.
[23] H. Kun, T. Haoran, C. Guojun, M. Dongdong, H. Kai, L. Lulu, W. Fengyun, Research on the dynamic fracture characteristics and constitutive model of cement-metakaolin stabilized soil under freeze-thaw cycle conditions, Constr. Build. Mater. 481 (2025) 141641.
[24] A.G. Alareqi, J. Gu, A.L.W. Ibrahim, E.E. Nyakilla, A. Salah, G. Al-khulaidi, Enhancing the durability of oil and gas wells using metakaolin-modified cement: An investigation of compressive and shear bond strengths at 95 and 180 °C, Constr. Build. Mater. 458 (2025) 139572.
[25] R. Fernandez, F. Martirena, K.L. Scrivener, The origin of the pozzolanic activity of calcined clay minerals: A comparison between kaolinite, illite and montmorillonite, Cem. Concr. Res. 41 (1) (2011) 113–122.
[26] Q. Huang, Q. Wang, Z. Zhang, C. Shen, W. Zhou, X. Xu, X. Zhu, Effect of metakaolin fineness on performance and microstructure of cement-based materials, J. Build. Eng. 99 (2025) 111577.
[27] C. Liang, Y. Xing, X. Hou, Multi-scale study on mechanical performance optimization mechanisms of aeolian sand cement-based materials incorporating discarded mask fibres and metakaolin, Constr. Build. Mater. 470 (2025) 140653.
[28] H. El-Diadamony, A.A. Amer, T.M. Sokkary, S. El-Hoseny, Hydration and characteristics of metakaolin pozzolanic cement pastes, HBRC J. 14 (2) (2018) 150–158.
[29] H.S. Al-alaily, A.A.A. Hassan, Time-dependence of chloride diffusion for concrete containing metakaolin, J. Build. Eng. 7 (2016) 159–169.
[30] R. Siddique, J. Klaus, Influence of metakaolin on the properties of mortar and concrete: A review, Appl. Clay Sci. 43 (3) (2009) 392–400.
[31] H.-S. Kim, S.-H. Lee, H.-Y. Moon, Strength properties and durability aspects of high strength concrete using Korean metakaolin, Constr. Build. Mater. 21 (6) (2007) 1229–1237.
[32] A. Machner, M. Zajac, M. Ben Haha, K.O. Kjellsen, M.R. Geiker, K. De Weerdt, Stability of the hydrate phase assemblage in Portland composite cements containing dolomite and metakaolin after leaching, carbonation, and chloride exposure, Cem. Concr. Compos. 89 (2018) 89–106.
[33] R. Cai, Z. He, S. Tang, T. Wu, E. Chen, The early hydration of metakaolin blended cements by non-contact impedance measurement, Cem. Concr. Compos. 92 (2018) 70–81.
[34] O. Keleştemur, B. Demirel, Effect of metakaolin on the corrosion resistance of structural lightweight concrete, Constr. Build. Mater. 81 (2015) 172–178.
[35] V. Papp, I. Ardelean, A. Bulátkó, K. László, A. Csík, R. Janovics, M. Kéri, Effect of metakaolin and fly ash on the early hydration and pore structure of Portland cement, Cem. Concr. Res. 196 (2025) 107928.
[36] N. Ulloa, E. Zumba, M. Albuja, D. Mayorga, Modeling the Compressive Strength of Metakaolin-Based Self-Healing Geopolymer Concrete Using Machine Learning Models, Civil. Eng. J. 11 (2025) 1596–1623.
[37] N. Saboo, S. Shivhare, K.K. Kori, A.K. Chandrappa, Effect of fly ash and metakaolin on pervious concrete properties, Constr. Build. Mater. 223 (2019) 322–328.
[38] J. Qian, M. Song, L. Jian-zhong, S. Liang, Effect of Adding Limestone on the Physical,Mechanical and Microstructural Properties of Alumino-silicate Geopolymer, Bull. Chin. Ceram. Soc. 35 (03) (2016) 875–878+883.
[39] K. De Weerdt, K.O. Kjellsen, E. Sellevold, H. Justnes, Synergy between fly ash and limestone powder in ternary cements, Cem. Concr. Compos. 33 (1) (2011) 30–38.
[40] Y. Li, X. Zeng, X. He, G. Long, J. Wang, L. Zeng, Effects of paraffin, metakaolin, and steam curing regimes on the electrical resistivity of steam-cured cement-based materials, Constr. Build. Mater. 458 (2025) 139615.
[41] R.G. Navarro-Leal, O. Burciaga-Díaz, J. Rodríguez-Morales, J.I. Escalante-García, Eco-efficient ternary cements with limestone powder, metakaolin and recycled waste glass: Characterization and sustainability assessment, Constr. Build. Mater. 479 (2025) 141432.
[42] Q. Qin, Q. Meng, M. Gan, J. Zhang, P. Yi, Synergistic effects of waste coral powder and metakaolin in cement pastes: Hydration, pore structure, rheology, and strength, J. Build. Eng. 97 (2024) 111001.

[43] Q. Li, Y. Fan, Y. Zhao, H. Chen, S.P. Shah, AC impedance spectroscopy interpretation of the hydration behavior for cement mortar containing fly ash and nano-metakaolin, Constr. Build. Mater. 468 (2025) 140436.
[44] M. Sun, S. Zhang, Y. Fan, J. Zheng, Acoustic emission study on the fracture process of fly ash-nano-metakaolin cement mortar under composite salt dry and wet cycles, J. Build. Eng. 108 (2025) 112829.
[45] M. Antoni, J. Rossen, F. Martirena, K. Scrivener, Cement substitution by a combination of metakaolin and limestone, Cem. Concr. Res. 42 (12) (2012) 1579–1589.
[46] J. Tang, S. Wei, W. Li, S. Ma, P. Ji, X. Shen, Synergistic effect of metakaolin and limestone on the hydration properties of Portland cement, Constr. Build. Mater. 223 (2019) 177–184.
[47] R. Bucher, P. Diederich, G. Escadeillas, M. Cyr, Service life of metakaolin-based concrete exposed to carbonation: Comparison with blended cement containing fly ash, blast furnace slag and limestone filler, Cem. Concr. Res. 99 (2017) 18–29.
[48] Y. Bailian, W. Leichong, S. Zhonghe, Y. Rui, G. Xu, Rebar-Protecting Properties of Limestone Powder-Metakaolin Cementitious Materials System under Seawater-Freshwater Intermixed Environment, Bull. Chin. Ceram. Soc. 39 (10) (2020) 3244–3251.
[49] K. Vance, M. Aguayo, T. Oey, G. Sant, N. Neithalath, Hydration and strength development in ternary portland cement blends containing limestone and fly ash or metakaolin, Cem. Concr. Compos. 39 (2013) 93–103.
[50] Z. Long, G. Long, Z. Tang, M. Shangguan, J. Wang, M. Yi, Y. Zhang, L. Peng, L. Wang, Analysis of hydration kinetics in high early-strength cementitious system with calcium sulphoaluminate cement and CSH seeds, Constr. Build. Mater. 448 (2024) 138222.
[51] J. Zelić, D. Rušić, D. Veža, R. Krstulović, The role of silica fume in the kinetics and mechanisms during the early stage of cement hydration, Cem. Concr. Res. 30 (10) (2000) 1655–1662.
[52] H. Zhang, Z. Yang, Y. Su, Hydration kinetics of cement-quicklime system at different temperatures, Thermochim. Acta 673 (2019) 1–11.
[53] M. Muhsin, Advances in Concrete Technology Based on New Materials and Applications, KHWARIZMIA 2024 (2024) 63–73.
[54] G.W. Scherer, J. Zhang, J.J. Thomas, Nucleation and growth models for hydration of cement, Cem. Concr. Res. 42 (7) (2012) 982–993.
[55] S.Ao China, GB 175-2023 Commen Portland Cement, Standalisation Administration of China, 2023.
[56] P. Zhan, J. Xu, J. Wang, C. Jiang, Multi-scale study on synergistic effect of cement replacement by metakaolin and typical supplementary cementitious materials on properties of ultra-high performance concrete, Constr. Build. Mater. 307 (2021) 125082.
[57] S.Ao China, GB/T 14684-2022 Sand for construction, Standardisation Administration of China, 2022.
[58] S.Ao China, GB 8077-2023 Test method for the homogeneity of Cementitious mixtures, Standalisation Administration of China, 2023.
[59] W. Huang, H. Kazemi-Kamyab, W. Sun, K. Scrivener, Effect of cement substitution by limestone on the hydration and microstructural development of ultra-high performance concrete (UHPC), Cem. Concr. Compos. 77 (2017) 86–101.
[60] A. Tironi, A.N. Scian, E.F. Irassar, Blended cements with limestone filler and kaolinitic calcined clay: Filler and pozzolanic effects, J. Mater. Civil. Eng. 29 (9) (2017) 04017116.
[61] Z. Hu, S. Guo, H. Zhu, J. Xu, X. Dai, Q. Chen, Z. Jiang, H. Zhu, Synergetic effect of C-S-H seeds and SAP on LC3 UHPC: Microstructure evolution, compressive strength and autogenous shrinkage, J. Clean. Prod. 502 (2025) 145364.
[62] S. Cheng, K. Chen, X. Chen, Y. Zuo, J.-X. Lu, Insight into the mechanism of sulfate and magnesium ions on chloride diffusion and phase assemblage in limestone calcined clay cement (LC3), Cem. Concr. Compos. 162 (2025) 106147.
[63] Z. Huang, T. Liang, L. Chen, Experimental studies on durability performances of ultra-lightweight low-carbon LC3 cement composites against chloride ingression and carbonation, Constr. Build. Mater. 395 (2023) 132340.
[64] M. Thomas, R. Hooton, A. Scott, H. Zibara, The effect of supplementary cementitious materials on chloride binding in hardened cement paste, Cem. Concr. Res. 42 (1) (2012) 1–7.
[65] M.J. DeJong, F.-J. Ulm, The nanogranular behavior of C-S-H at elevated temperatures (up to 700 °C), Cem. Concr. Res. 37 (1) (2007) 1–12.
[66] P. Zhan, J. Wang, H. Zhao, W. Li, S.P. Shah, J. Xu, Impact of synthetic C-S-H seeds on early hydration and pore structure evolution of cement pastes: A study by 1H low-field NMR and path analysis, Cem. Concr. Res. 175 (2024) 107376.
[67] J. Xu, P. Zhan, W. Zhou, J. Zuo, S.P. Shah, Z. He, Design and assessment of eco-friendly ultra-high performance concrete with steel slag powder and recycled glass powder, Powder Technol. 419 (2023) 118356.
[68] J.A. Bogas, A. Carriço, A.J. Tenza-Abril, Microstructure of thermoactivated recycled cement pastes, Cem. Concr. Res. 138 (2020) 106226.
[69] P. Zhan, J. Xu, J. Wang, J. Zuo, Z. He, Structural supercapacitor electrolytes based on cementitious composites containing recycled steel slag and waste glass powders, Cem. Concr. Compos. 137 (2023) 104924.
[70] A. Valori, P.J. McDonald, K.L. Scrivener, The morphology of C–S–H: Lessons from 1H nuclear magnetic resonance relaxometry, Cem. Concr. Res. 49 (2013) 65–81.
[71] P.J. McDonald, V. Rodin, A. Valori, Characterisation of intra- and inter-C–S–H gel pore water in white cement based on an analysis of NMR signal amplitudes as a function of water content, Cem. Concr. Res. 40 (12) (2010) 1656–1663.
[72] J.J. Thomas, A new approach to modeling the nucleation and growth kinetics of tricalcium silicate hydration, J. Am. Ceram. Soc. 90 (10) (2007) 3282–3288.
[73] Z. Zhang, P. Yan, Hydration kinetics of the epoxy resin-modified cement at different temperatures, Constr. Build. Mater. 150 (2017) 287–294.
[74] G. Long, Y. Li, C. Ma, Y. Xie, Y. Shi, Hydration kinetics of cement incorporating different nanoparticles at elevated temperatures, Thermochim. Acta 664 (2018) 108–117.
[75] H. Zhang, X. Liu, P. Feng, L. Li, W. Wang, Influence of temperature rising inhibitor on nucleation and growth process during cement hydration, Thermochim. Acta 681 (2019) 178403.
[76] J. He, G. Long, K. Ma, Y. Xie, Influence of fly ash or slag on nucleation and growth of early hydration of cement, Thermochim. Acta 701 (2021) 178964.
[77] J.J. Thomas, H.M. Jennings, J.J. Chen, Influence of Nucleation Seeding on the Hydration Mechanisms of Tricalcium Silicate and Cement, J. Phys. Chem. C. 113 (11) (2009) 4327–4334.
[78] M. Zong-yun;, L. Yi-liang;, W. Da-guang;, L. Zong-jie;, B. Li-gai, Research Progress on the Physical Properties of Cement-Based Materials Blended with Metakaolin, Bull. Chin. Ceram. Soc. 37 (03) (2018) 911–917.
[79] X. Chun-lei;, Z. Hong-wei;, Z. Xiao-liang;, L. Zhen-zheng, Effects of Component Admixtures Based on Fly Ash,Metakaolin and Limestone Powder on Microstructure and Early Age Shrinkage of Concrete, Bull. Chin. Ceram. Soc. 36 (09) (2017) 3075–3081.
[80] L. Duyou, Z. Shaohua, X. Jiangtao, L. Kang, X. Zhongzi, Effects of Limestone Powder and Metakaolin on Strength and Hydration Assemblages of Blended Cements, J. Chin. Ceram. Soc. 45 (5) (2017) 662–667.
[81] F. Yonghao, Z. Bo, Z. Yitao, METAKAOLIN AND ITS APPLICATION IN HIGH PERFORMANCE CONCRETE, Bull. Chin. Ceram. Soc. 31 (8) (2003) 801–805.
[82] K. Sotiriadis, A.S. Mazur, P.M. Tolstoy, P. Mácová, A. Viani, External magnesium sulfate attack on hydrated Portland-limestone cements: Effect of the concurrent presence of sodium chloride in the corrosive environment and metakaolin admixture in the binder, Cem. Concr. Compos. 151 (2024) 105614.